Pattern Recognition 124 (2022) 108463

Contents lists available at ScienceDirect

Pattern Recognition

journal homepage: www.elsevier.com/locate/patcog

A new framework of designing iterative techniques for image deblurring

Min Zhang[a], Geoffrey S. Young[b], Yanmei Tie[d], Xianfeng Gu[c], Xiaoyin Xu[b,*]

[a] Collabrative Innovation Center of Artificial Intelligence, College of Computer Science and Technology, Zhejiang University, Hangzhou, Zhejiang 310027, China
[b] Departments of Radiology, Brigham and Women's Hospital and Harvard Medical School, Boston, MA 02115, USA
[c] Department of Computer Science, Stony Brook University, Stony Brook, NY 11794, USA
[d] Department of Neurosurgery, Brigham and Women's Hospital, Harvard Medical School, Boston, MA 02115, USA

ARTICLE INFO

Article history:
Received 6 January 2021
Revised 22 November 2021
Accepted 26 November 2021
Available online 27 November 2021

Keywords:
Continuous forward model update
GMRES
Inverse problem
Image deblurring
Iterative algorithms
Landweber method
Least square method
Van Cittert method

ABSTRACT

In this work we present a framework of designing iterative techniques for image deblurring in inverse problem. The new framework is based on two observations about existing methods. We used Landweber method as the basis to develop and present the new framework but note that the framework is applicable to other iterative techniques. First, we observed that the iterative steps of Landweber method consist of a constant term, which is a low-pass filtered version of the already blurry observation. We proposed a modification to use the observed image directly. Second, we observed that Landweber method uses an estimate of the true image as the starting point. This estimate, however, does not get updated over iterations. We proposed a modification that updates this estimate as the iterative process progresses. We integrated the two modifications into one framework of iteratively deblurring images. Finally, we tested the new method and compared its performance with several existing techniques, including Landweber method, Van Cittert method, GMRES (generalized minimal residual method), and LSQR (least square), to demonstrate its superior performance in image deblurring.

1. Introduction

In many imaging applications, including medicine and biology [1,2], optics [3,4], remote sensing [5], astrophysics [6], and other fields [7], due to the relative motion between objects and the imaging device [8], observed images are blurred and often contaminated by measurement noise. Image quality may also be affected by packet loss due to the channel impairment during transmission [9,10]. Restoration of images is also necessary in compressed sensing in that one needs to solve an under-determined problem [11,12]. To restore the original images from the smoothed observations, we can employ either direct inversions or iterative solutions. Typical direct inversions include truncated singular value decomposition (SVD) inversion [13,14], Tikhonov regularization [15], total variation regularization [16,17] and others. Representative iterative solutions include Landweber method [18], Van Cittert method [19], conjugate gradient descent [20], Kalman filter-type method [21], and others [22–24]. For both types of approaches, maintaining the stability of the inversion process is critical to obtain reasonable results. However, a trade-off exists between maintaining stability and achieving a satisfactory level of accuracy in results. In direct inversion methods, the trade-off manifests as the selection of the number of singular values in truncated SVD inversion or the weight factor in Tikhonov-like regularization [25]. In iterative inversion methods, the trade-off manifests as the selection of the iterative step size and the threshold used in stopping the iteration. In addition to the above two general types of methods, hybrid techniques have also been proposed to solve ill-posed problems. For example, in a hybrid setup, an inversion problem may be approximated by a series of small bidiagonal systems to be solved via the Lanczos process [26]. In addition to the direct and iterative methods, in recent years other types of methods have been proposed. For example, Singha and Majumdar presented a method that treats inverse problems as a domain adaptation in a coupled dictionary learning setup [27]. Peng et al. proposed a method employing two-dimensional principal component analysis in two directions to extract feature-based sparse representation prior in a feature space instead of in the pixel space given by a blurred image, thus mitigating the effect of blurring [28]. In recent years, deep learning techniques have also been proposed to solve inverse problems. For example, Chun et al. presented an iterative neural network approach that combines regression neural network with an iterative reconstruction algorithm to recon-

* Corresponding author.
E-mail address: xxu@bwh.harvard.edu (X. Xu).

https://doi.org/10.1016/j.patcog.2021.108463
0031-3203/

struct images [29]. In their approach, called Momentum-Net, momentum terms are used in the extrapolation modules and majorizers are used in non-iterative model-based image reconstruction modules to obtain fast convergence rate and accurate results. Liu et al. proposed a method to adaptively guide the trajectories of learning-based iterations to restore blurred images in an unrolling optimization framework [30], where unrolling refers to the phenomenon that one can unroll an iterative method to become a feed-forward network. A potential limitation of unrolling iterative methods, however, is that the structure of resulting neural network may be highly complicated [31].

In this work, we focused on the Landweber method as it is a widely used technique and has motivated many variations of the original design, such as the smoothed-project Landweber method used in compressive sensing [32], the Runge–Kutta type modification whereby a 2-stage Runge–Kutta solution is applied to Landweber-like iteration [33], relaxation whereby an iterative relaxation strategy is used to accelerate the convergence [34], and the reduced-base method that couples the usually high-dimensional parameter spaces in the inverse problem with the adaptive online reduced basis updates to achieve faster convergence [35]. In addition, many derivatives of Landweber methods have been developed for image deblurring [36–38]. Here, we presented a new thought on designing iterative techniques that can perform better in many scenarios, especially in restoring the high-frequency components of images. There are two new ideas in our proposed method. For the first idea, we observed that the iterations of Landweber method can be decomposed into two terms, whereby the first term is a constant that remains unchanged throughout the iterations, and the second term is being updated each time. For the method to restore a blurred image, it requires the two terms to work together to generate a satisfactory result. Detailed analysis showed that the first term is a twice low-pass filtered version of the true image, meaning that the first term is of very low-frequency (or even smoother than the observed image). For the whole method to generate good results, the second term then needs to cancel out the low-frequency components in the much smoothed first term, a task that often is challenging. We therefore propose to modify the first term so that it is just a one-time low-pass filtered version of the true image.

For the second idea, we observed that, in iterative methods like the Landweber method, the whole iterative process hinges on the original inverse problem, starting with the blurred observation as the best estimate of the true image, and then it tries to approximate the true image iteratively by minimizing a cost function. We argue that we can obtain better results in designing iterative techniques by using the up-to-date best estimate of the true image at each iteration and solving a "new" inverse problem every time. In other words, for the very first iteration, our best estimate of the true image is indeed the blurred observation. However, starting with the second iteration, our best estimate of the true image is the restoration result given by the first iteration. So, for the second iteration, we can use the output of the first observation as the starting point to compute the output of the second iteration. The same process can then be repeated for the subsequent iterations. In this way, we should obtain better performance in the whole process. In this paper, we, therefore, have presented our new designs of iterative techniques by incorporating the above ideas.

The paper is organized as follows. In Section 2 we have explained the motivation of our idea and described the design of new method by using Landweber method as the starting point. In Section 3 we used test images to evaluate and compare the new method with the standard Landweber method, Van Cittert method, GMRES, and LSQR. We have discussed observations about the new method and offered conclusions in Section 4.

2. Method

In a typical setup of image deblurring, we assume that the observed image g is a blurred version of true image f, plus some measurement noise w, such that we have an inverse problem

$$g = Hf + w \tag{1}$$

where H is the point spread function (PSF) and we need to find f. In the blurring process, the effect of H can be considered as a low-pass filter such that it smooths a sharp image f to generate g. In Landweber method, to find a solution f to Eq. (1), we look to minimize

$$\text{argmin} J(f) = \frac{1}{2}||Hf - g||_2^2 \tag{2}$$

Take the derivative of the above formula, we have

$$\nabla J(f) = H^T(Hf - g) \tag{3}$$

Then by gradient descent, Landweber method iteratively solves Eq. (2) by

$$f^{n+1} = f^n - \beta \nabla J(f) \tag{4}$$

We initialize f^0 to the observation g, and, for the first few iterations, the Landweber method has the form of

$$f^0 = g \tag{5}$$

$$f^1 = f^0 + \beta H^T(g - Hf^0) = \beta H^T g + (f^0 - \beta H^T H f^0) \tag{6}$$

$$\vdots$$

$$f^{n+1} = f^n + \beta H^T(g - Hf^n) = \beta H^T g + (f^n - \beta H^T H f^n) \tag{7}$$

$n = 1, 2, \ldots$ for iteration $n+1$, where β is a small positive constant controlling the speed of iteration and superscript T stands for transpose. To ensure the stability of the iterative process, β must be less than $\frac{2}{\lambda_1^2}$ where λ_1 is the largest singular value of H. In implementation, the calculation of singular values takes a long time for large matrices and, without knowing the specific range for β, it is prudent to select a small β. However, the downside of choosing a small β is that the convergence will take a long time. In calculation, the Landweber method is implemented in the lexicographic manner such that f and g become column vectors, instead of matrices. Overall, the purpose of the Landweber method is to recover the sharp image f from its low-pass filtered version g.

From Eq. (7), we note that the first term $\beta H^T g$ on the right-hand side (RHS) is a constant vector while only the second term $(f^n - \beta H^T H f^n)$ is updated in the iterations. Examining the iterative process of Eq. (7), especially its first term $\beta H^T g$ on the RHS, we can make two observations and, based on the two observations, we propose two changes to the iterative solution.

2.1. First observation and the proposed change

The first observation is that, for the first term $\beta H^T g$ on the RHS of Eq. (7), β is a scalar constant, H^T is a low-pass filter, and g is a smoothed version of f. Then the effect of $H^T g$ is to essentially low-pass filter g again, further shifting the frequencies of g down to low-frequency and making g even smoother. Fig. 1 shows what image f, its observed image g which equals to $Hf + w$ and the further blurred image $H^T g$ may look like. For this example, the true image was blurred by a Gaussian kernel with a bandwidth of 7 and a standard deviation of 1.0.

In this particular example, we can see that, while g is a blurred version of f, some details are still discernible. However,

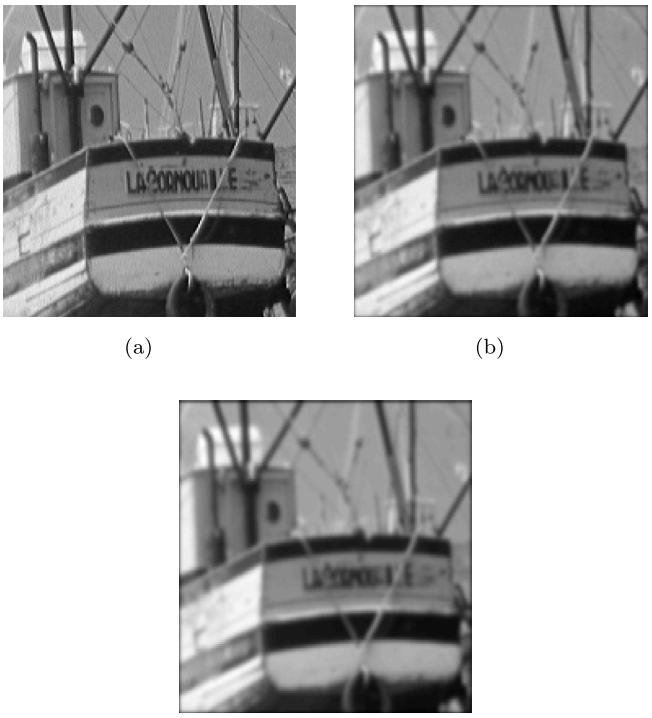

Fig. 1. (a) True f of part of the "boat" image. (b) Blurred observation g. (c) Further blurred image $H^T g$.

$H^T g$ is even more blurred than g, making many details unreadable. Given a deblurring approach, under the same condition, it is likely more difficult to recover f from $H^T g$, which is used in the standard Landweber method, than from g. To find f, then Landweber method relies on the second term $(f^n - \beta H^T H f^n)$ to not only recover the lost high-frequency components of f, but also to cancel out the low-frequency components in $H^T g$. Therefore, it seems reasonable that, if we remove H^T in the first term on the RHS, we can reduce the burden placed on the second term on the RHS to accelerate the iterative process to find f. In other words, the iterative process can be tentatively designed as

$$f^0 = g \tag{8}$$

$$f^1 = \beta g + (f^0 - \beta H^T H f^0) \tag{9}$$

$$\vdots$$

$$f^{n+1} = \beta g + (f^n - \beta H^T H f^n) \tag{10}$$

for $n = 1, 2, \ldots$, so g in the first term on the RHS is not low-pass filtered by H^T. Here we note that, though Eq. (10) is not directly derived from minimizing the cost of Eq. (2), it can lead to superior computational results in restoration. As we will see next, the iterative process of Eq. (10) can be further optimized.

2.2. Second observation and the proposed change

The second observation is that, from Eqs. (8) and (7), we note that g is used as the initial estimate for the true image f. This is a reasonable estimate because, without further computations, g is the best guess we have when the iterations start. If we use Eq. (10) to express the first iteration, we have

$$f^1 = \beta g + (f^0 - \beta H^T H f^0) \tag{11}$$

where g is the best estimate to be used to calculate f^1. Here we note that, in Eq. (11), f^0 is actually g, but for the convenience of discussion below, we keep the notion of f^0 in the second term. However, starting from the second iteration, our best estimate for the true f is no longer g but f^1 since f^1 now is available. If we assume f^1 is one-step closer to f than g, then we should replace g by f^1 so that, to obtain f^2, our best estimate for true image f now is f^1. In other words, we assume that, at the second iteration, we are faced with a "new" inverse problem, that is,

$$f^1 = Hf + w \tag{12}$$

because we now have f^1 available to us. Then our goal is to solve Eq. (12). Applying Eq. (11) to the new inverse problem of Eq. (12), the process of computing f^2 can be written as

$$f^2 = \beta f^1 + (f^1 - \beta H^T H f^1). \tag{13}$$

In other words, starting from the second iteration, we can replace g in Eq. (11) by the result of the previous iteration because, at each iteration, we have a new estimate that is better than g in terms of its distance to the true f. At the third iteration, our inverse problem becomes

$$f^2 = Hf + w \tag{14}$$

and our solution is similar to Eq. (13), that is,

$$f^3 = \beta f^2 + (f^2 - \beta H^T H f^2). \tag{15}$$

Essentially, the idea is that, as we progress through each iteration, we have an updated inverse problem and we solve the problem via one iteration, and then we move on to the next inverse problem and, again, solve it via one iteration. If we define

$$\Delta f^n \equiv f^n - \beta H^T H f^n \tag{16}$$

then we have

$$f^{n+1} = \beta f^n + \Delta f^n \tag{17}$$

while for the original Landweber method we have

$$f^{n+1} = \beta H g + \Delta f^n \tag{18}$$

2.3. The finalized new design

So, based on the above two observations, we propose a new iterative method as follows.

$$f^0 = g \tag{19}$$

$$f^1 = \beta g + (f^0 - \beta H^T H f^0) \tag{20}$$

$$f^2 = \beta f^1 + (f^1 - \beta H^T H f^1) \tag{21}$$

$$\vdots$$

$$f^{n+1} = \beta f^n + (f^n - \beta H^T H f^n) \tag{22}$$

for $n = 1, 2, \ldots$. In the new iterative method, the two changes are, (1) removal of PSF H in the first term on the RHS and (2) replacement of g by f^n for $n > 1$. The iteration stops when the difference between two consecutive results is smaller than a threshold or the number of iterations reaches a preset level. As discussed before, the new method implicitly assumes a new inverse problem starting with $n > 1$, whereas the inverse problem becomes $f^n = Hf^{(n-1)} + w$.

Computationally, we note that the new method has the similar complexity as the Landweber method as there are no extra operations. In addition, from Eq. (22), we note that the idea behind

the new method can be applied to other iterative algorithms because the proposed changes are about, first, how to prevent PSF H from low-pass filtering the already blurred observation g, and, second, how to utilize most recent intermediate results to update the inverse problem at each iteration. Note that the changes do not impact the second term on the RHS of the iterative process, which can be considered as how different methods calculate the stepwise changes to be added to the previous outputs. In other words, existing algorithms like the Landweber method solve one fixed inverse problem, as given by Eq. (1), in N iterations, while the new method solves N inverse problems in N iterations whereas each inverse problem is attempted only once. Our assumptions about admitting a solution is that f is smooth and H is Fréchet differentiable.

3. Results

In this section we evaluated the performance of the new method in deblurring. Because the new method is motivated by our observation of how then Landweber method proceeds, we compared the new method with the Landweber method. Also, because of the similarity between the Landweber method and Van Cittert method, which has the form of

$$f^{n+1} = \beta g + (f^n - \beta H f^n), \tag{23}$$

we included the Van Cittert method for comparison as well.

We used mean squared error (MSE), which is defined as

$$\text{MSE} = \frac{||f^n - f||_2^2}{L} \tag{24}$$

where L is the total number of pixels in an image, to evaluate the restoration. We also used structural similarity index measure (SSIM) [39] as a measurement of the quality of restoration. For two images u and v, SSIM is defined as

$$\text{SSIM} = \frac{(2\mu_u\mu_v + c_1)(2\sigma_{uv} + c_2)}{(\mu_u^2 + \mu_v^2 + c_1)(\sigma_u^2 + \sigma_v^2 + c_2)} \tag{25}$$

where μ_u and σ_u are the average and standard deviation of image u, respectively, and μ_v and σ_v are similarly defined for image v. In the definition, σ_{uv} is the covariance of u and v, and c_1 and c_2 are two positive numbers to ensure the stabilization of the division. For all the examples, signal-to-noise ratio (SNR) is defined as the energy of Hf over the energy of noise w

$$\text{SNR} = \log \frac{||Hf||_2^2}{||w||_2^2} \quad (dB) \tag{26}$$

where $||w||_2^2$ is the energy of the noise.

As the first example, we compared the three methods on deblurring the test image “baboon”. For this example, we set the Gaussian blurring kernel with a bandwidth of 7 and a standard deviation of 1.0. The SNR was 9.5 dB. We used a step size of 3e-4 for the iterative processes. Results are shown in Fig. 2. The original image and its blurred version are shown in Fig. 2(a) and (b). The restorations by the standard Landweber method, Van Cittert method, and the new method are shown in Fig. 2(c–e), respectively. From the three restorations, we note that the new method achieved the best performance as it showed more fine structure on the face and restored the pupil more sharply. The plot of MSEs in Fig. 2(f) showed that, in this example, the new method had the lowest MSE. We also computed the SSIMs of the three restorations corresponding to Fig. 2(c–e). The SSIMs were 0.6069, 0.6636, and 0.7463, respectively, indicating that the new method had the highest SSIM.

For the next example, we applied the three methods to deblur the “boat” image shown in Fig. 1(b). We set the step size to 1e-3 for the iterative processes. Results of the first 500 iterations are

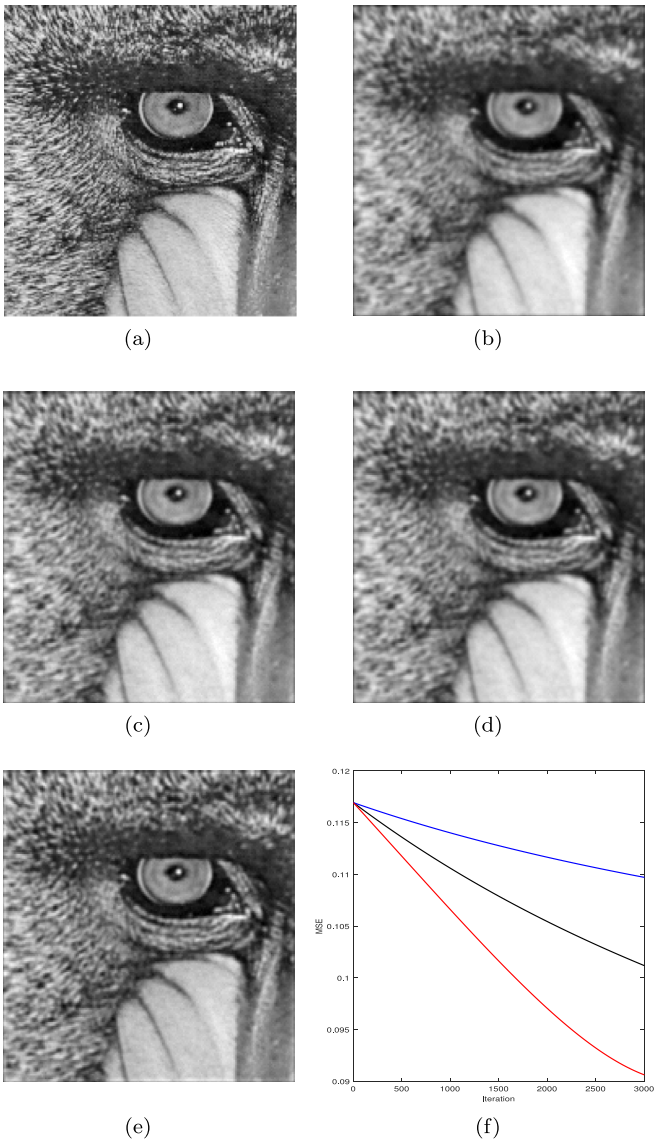

Fig. 2. (a) True image f. (b) Blurred observation g. (c) Restoration by Van Cittert method. (d) Restoration by Landweber method. (e) Restoration by the new method. (f) MSEs of the three methods. Black, Van Cittert method. Blue, Landweber method. Red, new method. (For interpretation of the references to color in this figure legend, the reader is referred to the web version of this article.)

shown in Fig. 3. It is observable that the new method gave the best result. The characters on the boat are more readable in Fig. 3(c) than in Fig. 3(a) and (b). Fig. 3(d) shows that the new method had lowest MSE. We calculated that the SSIMs of Fig. 3(a and b) were 0.6993, 0.7180, and 0.7462, respectively.

We then tested how the three methods performed if we increased the number of iterations to 1000. The results are shown in Fig. 4. From this figure, we observed that the MSE of the new method started to increase at iteration 800, yet its result was still sharper than those given by the other two methods. We calculated that the SSIMs of Fig. 4(a–c) were 0.7145, 0.7415, and 0.7756, respectively.

When we increased the number of iterations further to 1500, we obtained results shown in Fig. 5. It is interesting to note that the MSE of the new method exceeded those of the Van Cittert and Landweber methods. We calculated that the SSIMs of Fig. 5(a–c) were 0.7260, 0.7551, and 0.7318, respectively. Here we note that from the MSE plot and the SSIM calculation, it seems that the re-

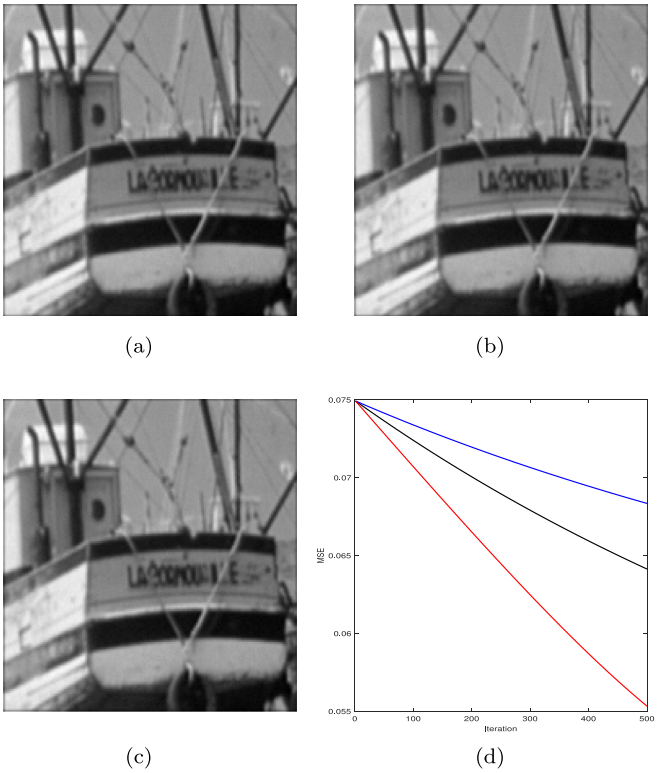

Fig. 3. (a) Restoration of Fig. 1 by Van Cittert method at 500 iterations. (b) Restoration by Landweber method at 500 iterations. (c) Restoration by the new method at 500 iterations. (d) MSEs of the three methods. Black, Van Cittert method. Blue, Landweber method. Red, new method. (For interpretation of the references to color in this figure legend, the reader is referred to the web version of this article.)

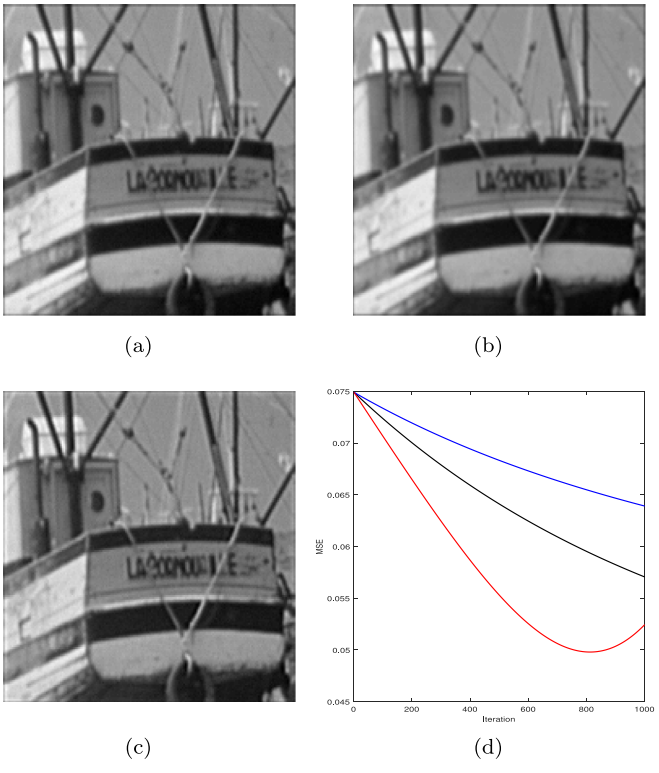

Fig. 4. (a) Restoration of Fig. 1 by Van Cittert method at 1000 iterations. (b) Restoration by Landweber method at 1000 iterations. (c) Restoration by the new method at 1000 iterations. (d) MSEs of the three methods. Black, Van Cittert method. Blue, Landweber method. Red, new method. (For interpretation of the references to color in this figure legend, the reader is referred to the web version of this article.)

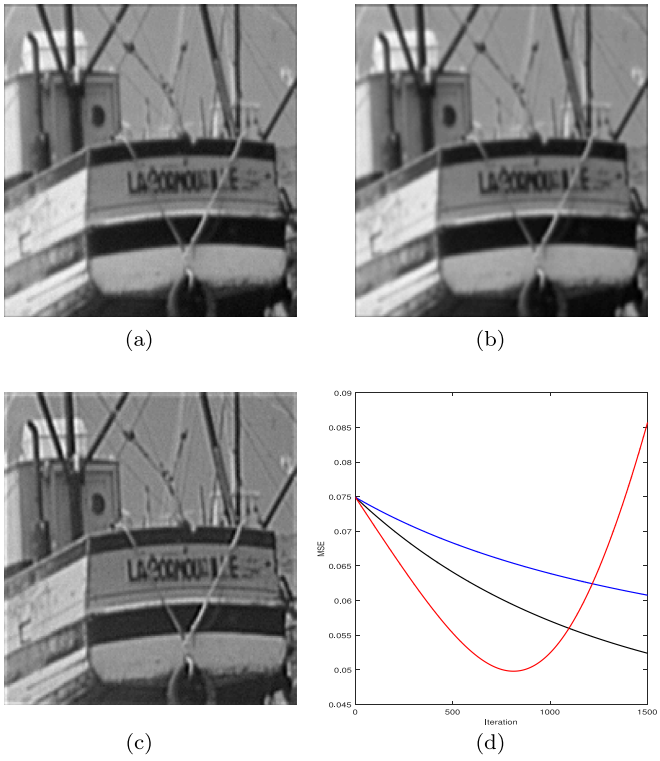

Fig. 5. (a) Restoration of Fig. 1 by Van Cittert method at 1500 iterations. (b) Restoration by Landweber method at 1500 iterations. (c) Restoration by the new method at 1500 iterations. (d) MSEs of the three methods. Black, Van Cittert method. Blue, Landweber method. Red, new method. (For interpretation of the references to color in this figure legend, the reader is referred to the web version of this article.)

sult of the new method was not as good as that of the Van Cittert method. Yet, from the restored images, we observed that the new method generated the sharpest result among the three methods. This phenomenon points to the fact that MSE and SSIM, though can measure difference between the true image and its restoration, do not always indicate whether the restoration is sharp or not.

As another example, we used a Gaussian kernel with a bandwidth of 3 and a standard deviation of 0.75 to blur a test image “sails” and added white Gaussian noise to the blurred image. The SNR was 9.4 dB. We then tested the Landweber method, Van Cittert method, and the new method on deblurring the image by 5000 iterations. The step size was set to 3e−4. Results and the MSEs are shown in Fig. 6. From the images, we see that the new method created a sharper restoration, such as the numbers on the sails, even when it had a larger MSE than the other two methods. From the MSE plot, it is also seen that the new method had a smaller error. It is interesting to note that the results of the new method and the Landweber method had similar MSEs, yet the result of the new method was sharper. The SSIMs of the standard Landweber method, Van Cittert method, and the new method were 0.8506, 0.8815, and 0.9200, respectively.

We next used the same blurring kernel and parameters and applied the three methods on test image “clock”. Results are shown in Fig. 7. We had the same observation that the new method generated a sharper result, despite that its MSE was higher than those of the other two methods. We also computed the SSIMs for Fig. 7(c–e) and they were 0.6389, 0.6236, and 0.6132, respectively. In this example, we have the same observation that it seemed the new method gave a result with a higher MSE and lower SSIM than the other two methods. Yet, visual inspection of the results indicated that the new method created sharpest restoration.

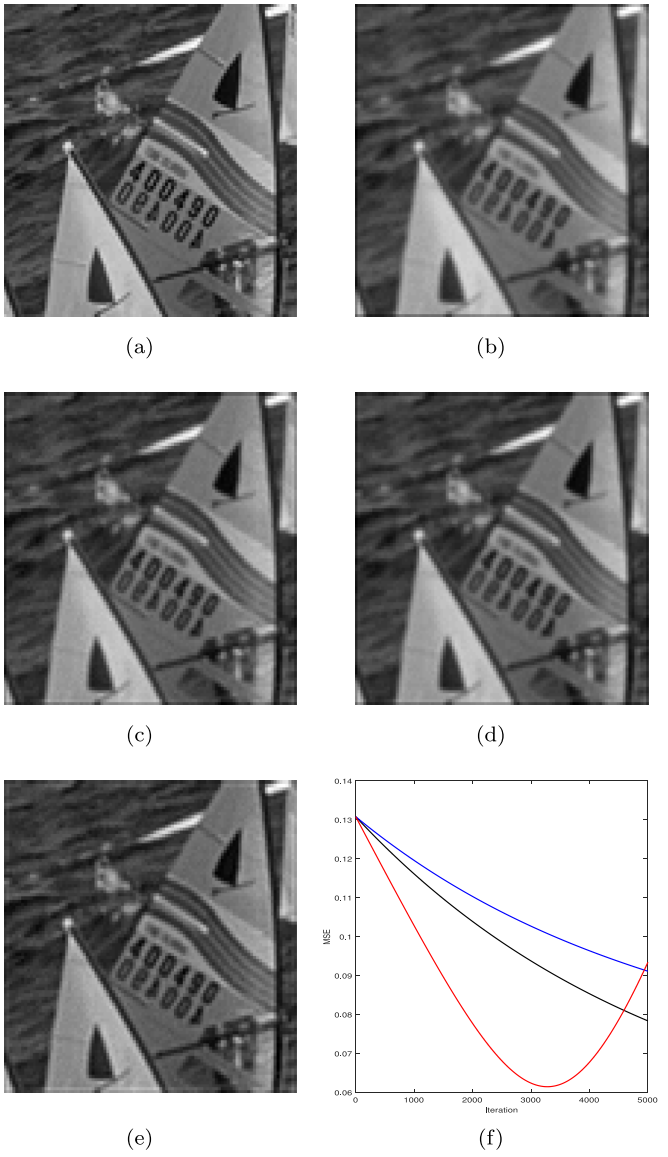

Fig. 6. (a) True image f. (b) Blurred observation g. (c) Restoration by Van Cittert method. (d) Restoration by Landweber method. (e) Restoration by the new method. (f) MSEs of the three methods. Black, Van Cittert method. Blue, Landweber method. Red, new method. (For interpretation of the references to color in this figure legend, the reader is referred to the web version of this article.)

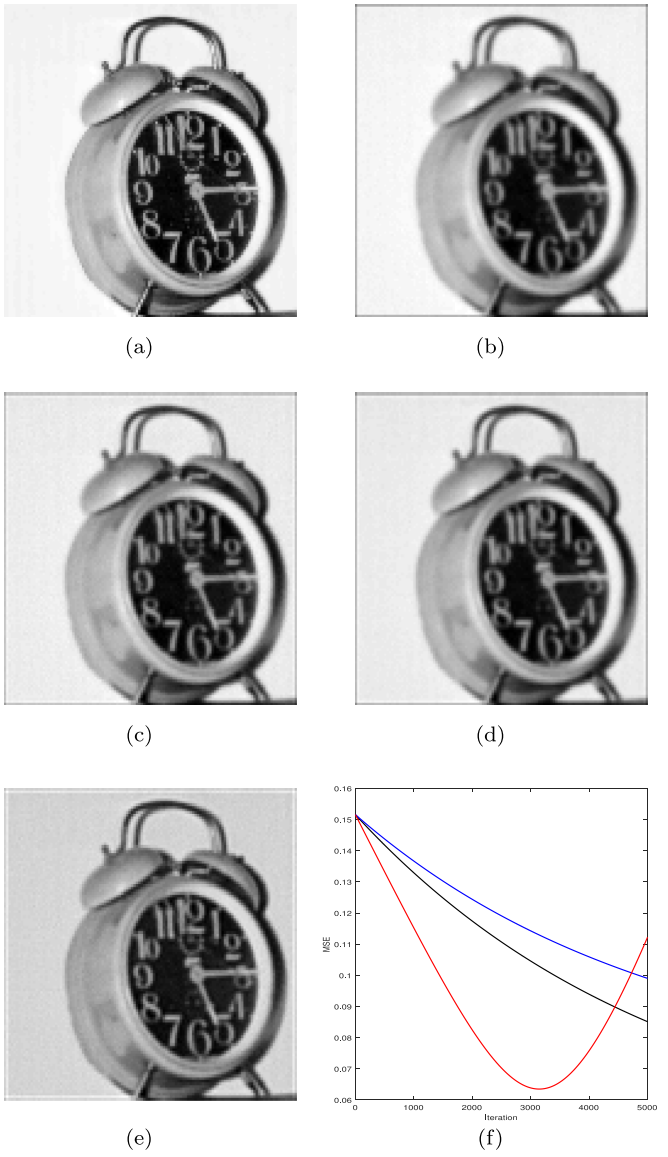

Fig. 7. (a) True image f. (b) Blurred observation g. (c) Restoration by Van Cittert method. (d) Restoration by Landweber method. (e) Restoration by the new method. (f) MSEs of the three methods. Black, Van Cittert method. Blue, Landweber method. Red, new method. (For interpretation of the references to color in this figure legend, the reader is referred to the web version of this article.)

Another scenario we tested is when the true PSF H is not known exactly. In the next example, we evaluated how the new method may perform using an estimated H to restore images. For the first example, the "bridge" image was blurred by a Gaussian kernel H with a bandwidth of 3 and a standard deviation of 1.0. The SNR was 9.8 dB. Assuming that we did not know H exactly, we used an estimate $\hat{H}$ with a bandwidth of 5 and a standard deviation of 1.5 to deblur the image. Results are shown in Fig. 8. We see from the comparison that the new method generated the best restoration as the restoration was sharper and showed more details about the "bridge". It also had a lower MSE. The SSIMs of Fig. 8(c–e) were 0.6988, 0.7810, and 0.7915, respectively.

Next we used several other test images for comparison among the three methods with different degrees of blurriness. These test images are shown in Fig. 9, downloaded from homepages.cae.wisc.edu/ece533/images/. Table 1 compares results given by the three methods on images blurred by a Gaussian kernel with a bandwidth of 3 and standard deviation of 1.0. The step size of restoration was 2e−4 and the number of iterations was 3000. Results in the table are given as MSE followed by SSIM. From the table we see that the new method achieved lower MSEs and higher SSIMs than the other two methods.

We next made the blurring effect more severe by increasing the standard deviation of the Gaussian kernel to 1.5 but kept all

Table 1
MSEs and SSIMs of the three methods in restoring images blurred by a Gaussian kernel with bandwidth of 3 and a standard deviation of 1.0. Numbers are MSE followed by SSIM, separated by "/".

	SNR	Landweber	Van Cittert	New
Tulips	8.7	0.187 / 0.851	0.168 / 0.869	0.066 / 0.900
Monarch	8.8	0.211 / 0.878	0.190 / 0.897	0.080 / 0.933
Gold hill	5.5	0.076 / 0.624	0.074 / 0.636	0.067 / 0.664
Saturn	8.5	0.161 / 0.885	0.145 / 0.882	0.048 / 0.886
Fruits	9.9	0.334 / 0.816	0.301 / 0.817	0.091 / 0.824
Mountain	9.4	0.404 / 0.634	0.378 / 0.667	0.294 / 0.727

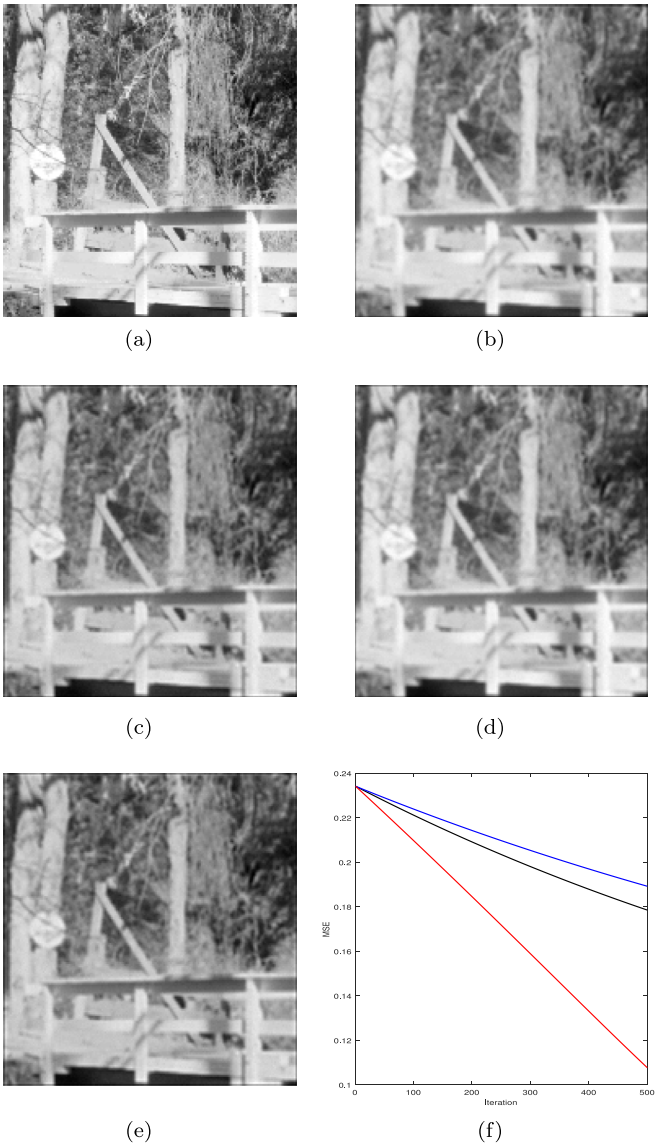

Fig. 8. (a) True image "bridge" f. (b) Blurred observation g by a Gaussian kernel H with a bandwidth of 3 and a standard deviation of 1.0. (c) Restoration by Van Cittert method using a Gaussian kernel $\hat{H}$ with a bandwidth of 5 and a standard deviation of 1.5. (d) Restoration by Landweber method using $\hat{H}$. (e) Restoration by the new method using $\hat{H}$. (f) MSEs of the three methods. Black, Van Cittert method. Blue, Landweber method. Red, new method. (For interpretation of the references to color in this figure legend, the reader is referred to the web version of this article.)

Fig. 9. Test images. Top, from left to right, tulips, monarch, and gold hill. Bottom, Saturn, fruits, and mountain.

Table 2
Comparison of the three methods in restoring images blurred by a Gaussian kernel with bandwidth of 3 and a standard deviation of 1.5. Numbers are MSE followed by SSIM.

	SNR	Landweber	Van Cittert	New
Tulips	7.7	0.493 / 0.632	0.427 / 0.698	0.274 / 0.793
Monarch	7.9	0.541 / 0.622	0.468 / 0.701	0.304 / 0.820
Gold hill	4.5	0.121 / 0.470	0.111 / 0.497	0.090 / 0.550
Saturn	7.5	0.439 / 0.739	0.379 / 0.774	0.240 / 0.834
Fruits	9.0	0.924 / 0.673	0.798 / 0.708	0.503 / 0.763
Mountain	8.4	0.772 / 0.383	0.686 / 0.447	0.507 / 0.546

the other setup the same. The results are shown in Table 2, from which, again, we note that the new method had the lowest MSEs and highest SSIMs.

In real world, it is often the case that we do not know the blurring PSF exactly. Next, we evaluated the new method when we used an inexact PSF to deblur an image. In this example, we also compared the new method not only with the standard Landweber method and the Van Cittert method but also the GMRES (generalized minimal residual method) and LSQR (least squares) methods. At first, we blurred an image with a Gaussian kernel with a bandwith of 3 and a standard deviation of 1.25. The SNR was 7.8 dB. We then used a Gaussian kernel with a bandwidth of 3 and a standard deviation of 1.55 to restore the image. The results of five methods are shown in Fig. 10. For the first three methods, we ran iterations to 2000 as the MSEs for the Van Cittert and Landweber methods continued to decrease. For the GMRES and LSQR, we ran iterations to 100 as their MSEs started to increase after the first several iterations. For the Van Cittert method, standard Landweber method, and the new method, their restorations were the results of 2000th iteration. For the GMRES and LSQR methods, their restorations were the results of their second iteration, as both methods achieved their lowest MSEs at the second iteration, which can also be seen from Fig. 10. Comparing the restoration results, we see that, in the presence of noise and with an estimated PSF, the new method gave the sharpest restoration, for example, the numbers on the watch, among the five methods. Next, we used the same test image but assumed that the PSF was under-estimated by 0.5. The results given by GMRES, LSQR, and the new method are shown in Fig. 11. From the figure, we note that the new method still generated the best restoration and, in this case, had lowest MSE. The results given by the Van Cittert and Landweber methods are not shown but they had higher MSEs than the new method and blurrier restorations. We also computed the SSIMs for the standard Landweber method, the Van Cittert method, GMRES, LSQR, and the new method. The values were 0.4921, 0.4710, 0.0264, 0.0677, and 0.3518, respectively. We note that the new method had a higher SSIM than GMRES and LSQR methods but its SSIM was lower than those of the standard Landweber method and the Van Cittert method. However, visual inspection of the restored images indicates that the new method had the best result as it shows more fine details about the watch.

Additional results are given in supplement materials, in which we performed ablation tests of implementing one idea only and compared the performance with the full new method, and more comparisons between the new method and two other existing iterative methods, GMRES and LSQR, and evaluated the new method on how it performs on restoring images blurred by a uniform kernel.

4. Discussion and conclusions

In this work we presented a new framework on designing iterative techniques for image deblurring. We demonstrated the performance of the new framework using the Landweber method as

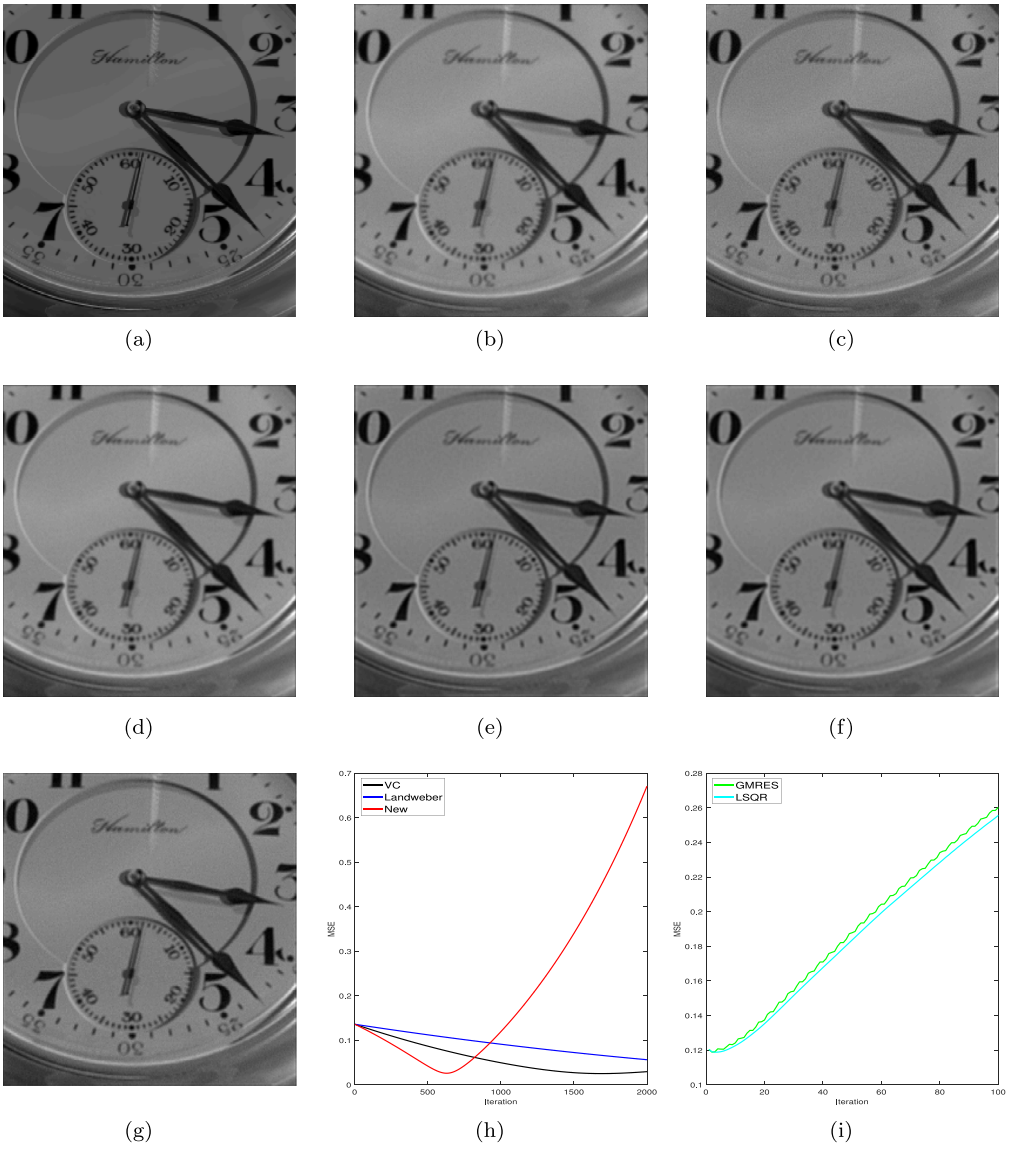

Fig. 10. (a) An original image. (b) Blurred observation. (c-g) Results by Van Cittert method, standard Landweber method, GMRES, LSQR, and the new method, respectively, when the PSF was not known exactly and its standard deviation was over-estimated by 0.3. The MSEs of the five restoration results were 0.0296, 0.0565, 0.1189, 0.1191, and 0.6712, respectively. (h) MSEs of the Van Cittert method, standard Landweber method, and new method. (i) MSEs of GMRES and LSQR methods.

Fig. 11. (a–c) Results by GMRES, LSQR, and the new method, respectively, when the PSF was not known exactly and its standard deviation was under-estimated by 0.5. The MSEs of the three restoration results were 0.1214, 0.1211, and 0.0940, respectively.

a baseline technique. The motivation for the new framework stems from two observations about the Landweber method.

The first observation is that, as the true images are degraded by the low-pass filtering effect of a PSF, it is reasonable to avoid using twice the low-pass filtered f from the beginning in the iterative process so the new method can achieve better performance. Our design was based on the idea of making the task of the iterative process easier because, as we showed, it is the iterative term that must cancel out the low-frequency components in the constant term to generate sharp restorations. If the constant term is much smoothed, as in the standard Landweber method, then the iterative term may not sufficiently cancel out the smoothness in the constant term, leading to sub-optimal results. Here we note that, for the image deblurring problem described in this work, we assumed an undetermined boundary condition. The reason is that, as shown by Zhou et al. [40], an undetermined boundary condition can lead to better results in image deblurring if the underlying image does not have high similarity at the boundary, which is the case for many images. On the other hand, if the underlying images have high similarity at the boundary, then a repeated boundary condition may lead to better results in deblurring [40]. In cases where a boundary condition can be imposed, Donatelli et al. proposed to replace the quadratic H^TH operator by $H'H$ where H' is the H related to the boundary conditions with the PSF rotated by 180 degrees and their results showed that re-blurring $H'H$ with anti-reflective boundary conditions can reduce the ringing effects during the blurring process [41]. Our method is distinct from the re-blurring idea by emphasizing the effect of avoiding two two times of low-pass filtering incurred by H^TH to reduce the burden for the deblurring process to generate sharp restorations.

The second observation is that we can treat each iteration as searching for solution to a new deblurring problem in the sense that, at each iteration, our best estimate about the true image is updated by the previous cycle and, therefore, we do not have to use the original blurry observation as our best estimate. In other words, traditional methods solve the inverse problem of $g = Hf + w$ over many iterations. In our proposal, we showed that it is beneficial to solve a series of inverse problems, starting with $g = Hf + w$, then the inverse problem is updated to $f^1 = Hf + w$, then to $f^2 = Hf + w$ and so on. For each updated inverse problem, we only solve it one time by $f^{n+1} = \beta f^n + (f^n - \beta H^T H f^n)$ where $n = 1, 2, \ldots$. Then the inverse problem gets updated and we then solve the "new" problem again.

The contribution of this work is two-fold. The first contribution is that it shows the initialization term in the Landweber method is a twice blurred version of true image f and it is beneficial to replace Hg with g to remove the additional low-pass filtering imposed by the PSF H. The second contribution is that, as we showed in the analysis of the iterative steps of Landweber method, we can update the inverse problem model as we progress through the iterations. Instead of keeping the inverse problem unchanged, meaning that we always start from the same point, we can update the inverse problem as we acquire an estimate of the true image. This estimate then can be used to rewrite the inverse problem and help the iterative process achieve a better performance. We note that the two contributions are not constrained to modifying the Landweber method. They are applicable to other iterative algorithms if they have the similar computational setup in initialization and updating the iterative process.

Here we note that we present the new framework as a standalone method, however, it is possible to integrate it with the latent iterative techniques it is based on. For example, it can be integrated with the standard Landweber method such that the new method is used for the first few hundreds of iterations while the standard Landweber method is used for the next several hundreds of iterations.

Based on the test results and comparisons, we can make several observations. First, it shows that the new method can generate sharper images as compared to other methods, whether its resulting images have a lower or higher MSE than the results given by the other two methods. This is likely due to the fact that the new method, using βg as the starting point, maintains more high-frequency components in the first place.

Second, when the PSF had to be estimated, the new method still generated the best results among the three methods, likely because of the constant part of the new iterative process, i.e., βg, is not filtered by the estimated PSF to start the iterations, thus reducing the impact of the imprecise PSF on the results.

It is also interesting to note that, as can be seen from our comparisons, MSE and SSIM do not always concur with visual inspection on how good a restored image is. Though a low MSE is typically desirable in image processing, depending on the underlying task of an application, a higher MSE may be an acceptable trade-off if the resulting image can provide useful information, such as in image deblurring. We used MSE in this work because the cost functions of many image deblurring algorithms essentially aims to minimize an energy term with an L_2 norm of the similar form as MSE, i.e., to minimize $||g - H\hat{f}||$ where $\hat{f}$ is the restored image. In our experiments, we note that a high SSIM is generally preferred but just relying on SSIM may lead to incorrect conclusion on selecting the best restoration results. This could be due to the fact that SSIM is not a parameter-free metric as the two constants c_1 and c_2 in Eq. (25) need to be carefully set to stabilize its calculation. To the best of our knowledge, there is no dedicated metric that assesses the quality of deblurred images in both a quantitative way that an algorithm can be based on and a qualitative way that agrees with visual inspection. It would be beneficial to develop such a metric, which, however, is beyond the scope of this work.

In this work, we compared the new method to the standard Landweber method, Van Cittert method, GMRES, and LSQR. We chose these methods for comparison because they constitute the backbone of many other methods and have broad practical applications. More importantly, the purpose of comparing the new method to these methods is to illustrate the impact of the idea on designing iterative deblurring algorithms to better recover the high-frequency components in images, which is the overarching goal of image deblurring. From the idea of constructing the new framework, the two novel modifications can be adapted to other iterative techniques in solving inverse problems, including but not limited to image deblurring.

There are limitations of this work. We derived the new design of the deblurring process via insights into the existing Landweber method to improve the performance of image deblurring, however, we did not theoretically analyze the convergent behavior of the new algorithm. Our numerical examples showed that the new algorithm can attain sharper restorations, though it may attain higher MSEs over an exceedingly large number of iterations. It points to the fact that a judiciously designed stopping rule is needed to stop the iterations. One choice is to stop the process when the difference between two iterations is smaller than a preset threshold.

Declaration of Competing Interest

Authors declare that they have no conflict of interest.

Acknowledgment

The work of X.X. was supported in part by NIH awards R01LM012434 and R01LM011415.

Supplementary material

Supplementary material associated with this article can be found, in the online version, at doi:10.1016/j.patcog.2021.108463.

References

[1] J. Poudel, Y. Lou, M.A. Anastasio, A survey of computational frameworks for solving the acoustic inverse problem in three-dimensional photoacoustic computed tomography, Phys. Med. Biol. 64 (14) (2019) 14TR01.
[2] R.A. Salido-Ruiz, R. Ranta, G. Korats, S. Le Cam, L. Koessler, V. Louis-Dorr, A unified weighted minimum norm solution for the reference inverse problem in EEG, Comput. Biol. Med. 115 (2019) 103510.
[3] E. Nepomnyashchaya, E. Velichko, E. Aksenov, Inverse problem of laser correlation spectroscopy for analysis of polydisperse solutions of nanoparticles, J. Phys. 769 (1) (2016) 012025.
[4] J.-L. Starck, Sparsity and Inv Prob in astrophysics, J. Phys. 699 (1) (2016) 012010.
[5] J. Wei, Y. Huang, K. Lu, L. Wang, Nonlocal low-rank-based compressed sensing for remote sensing image reconstruction, IEEE Geosci. Remote Sens. Lett. 13 (10) (2016) 1557–1561.
[6] S.H. Völkel, R. Konoplya, K.D. Kokkotas, Inverse problem for Hawking radiation, Phys. Rev. D 99 (10) (2019) 104025.
[7] C. Rawlings, C. Durkan, The inverse problem in magnetic force microscopy inferring sample magnetization from MFM images, Nanotechnology 24 (30) (2013) 305705.
[8] Y.-Q. Liu, X. Du, H.-L. Shen, S.-J. Chen, Estimating generalized gaussian blur kernels for out-of-focus image deblurring, IEEE Trans. Circuits Syst. Video Technol. 31 (3) (2020) 829–843.
[9] A. Akbari, M. Trocan, B. Granado, Sparse recovery-based error concealment, IEEE Trans. Multimed. 19 (6) (2017) 1339–1350.
[10] T.-H. Li, K.-S. Lii, A joint estimation approach for two-tone image deblurring by blind deconvolution, IEEE Trans. Image Proc. 11 (8) (2002) 847–858.
[11] A. Akbari, M. Trocan, Robust image reconstruction for block-based compressed sensing using a binary measurement matrix, in: 2018 25th IEEE International Conference on Image Processing (ICIP), IEEE, 2018, pp. 1832–1836.
[12] A. Akbari, D. Mandache, M. Trocan, B. Granado, Adaptive saliency-based compressive sensing image reconstruction, in: 2016 IEEE International Conference on Multimedia & Expo Workshops (ICMEW), IEEE, 2016, pp. 1–6.
[13] P.C. Hansen, The truncated SVD as a method for regularization, BIT Numer. Math. 27 (4) (1987) 534–553.
[14] P. Xu, Truncated SVD methods for discrete linear ill-posed problems, Geophys. J. Int. 135 (2) (1998) 505–514.
[15] P.C. Hansen, D.P. OLeary, The use of the L-curve in the regularization of discrete ill-posed problems, SIAM J. Sci. Comput. 14 (6) (1993) 1487–1503.
[16] S. Vatankhah, R.A. Renaut, V.E. Ardestani, Total variation regularization of the 3-D gravity inverse problem using a randomized generalized singular value decomposition, Geophys. J. Int. 213 (1) (2018) 695–705.
[17] M. Hintermüller, M. Holler, K. Papafitsoros, A function space framework for structural total variation regularization with applications in Inv Prob, Inverse Probl. 34 (6) (2018) 064002.
[18] L. Landweber, An iteration formula for Fredholm integral equations of the first kind, Am. J. Math. 73 (1951) 615–624.
[19] W. Layton, L. Rebholz, Approximate Deconvolution Models of Turbulence: Analysis, Phenomenology and Numerical Analysis, Springer-Verlag, Berlin, 2012.
[20] P. Concus, G.H. Golub, D.P. O'Leary, A generalized conjugate gradient method for the numerical solution of elliptic partial differential equations, in: Sparse Matrix Computations, Elsevier, 1976, pp. 309–332.
[21] F. Conte, A. Germani, G. Iannello, A Kalman filter approach for denoising and deblurring 3-D microscopy images, IEEE Trans. Image Proc. 22 (12) (2013) 5306–5321.
[22] A. Lucas, M. Iliadis, R. Molina, A.K. Katsaggelos, Using deep neural networks for Inv Prob in imaging: beyond analytical methods, IEEE Signal Process. Mag. 35 (1) (2018) 20–36.
[23] T. Tirer, R. Giryes, Image restoration by iterative denoising and backward projections, IEEE Trans. Image Proc. 28 (3) (2018) 1220–1234.
[24] T. Sun, R. Barrio, M. Rodríguez, H. Jiang, Inertial nonconvex alternating minimizations for the image deblurring, IEEE Trans. Image Proc. 28 (12) (2019) 6211–6224.
[25] M. Bertero, P. Boccacci, G. Desidera, G. Vicidomini, Image deblurring with Poisson data: from cells to galaxies, Inverse Probl. 25 (12) (2009) 123006.
[26] M. Hanke, On Lanczos based methods for the regularization of discrete ill–posed problems, BIT Numer. Math. 41 (5) (2001) 1008–1018.
[27] V. Singhal, A. Majumdar, A domain adaptation approach to solve inverse problems in imaging via coupled deep dictionary learning, Pattern Recognit. 100 (2020) 107163.
[28] J. Peng, Y. Shao, N. Sang, C. Gao, Joint image deblurring and matching with feature-based sparse representation prior, Pattern Recognit. 103 (2020) 107300.
[29] I.Y. Chun, Z. Huang, H. Lim, J. Fessler, Momentum-net: fast and convergent iterative neural network for inverse problems, IEEE Trans. Pattern Anal. Mach. Intell. (2020).
[30] R. Liu, S. Cheng, Y. He, X. Fan, Z. Lin, Z. Luo, On the convergence of learning-based iterative methods for nonconvex inverse problems, IEEE Trans. Pattern Anal. Mach. Intell. 42 (12) (2019) 3027–3039.
[31] G. Wang, J.C. Ye, B. De Man, Deep learning for tomographic image reconstruction, Nat. Mach. Intell. 2 (12) (2020) 737–748.
[32] M. Trevisi, A. Akbari, M. Trocan, Á. Rodrmíguez-Vázquez, R. Carmona-Galán, Compressive imaging using RIP-compliant CMOS imager architecture and landweber reconstruction, IEEE Trans. Circuits Syst. Video Technol. 30 (2) (2019) 387–399.
[33] W. Wang, B. Han, L. Li, A Runge–Kutta type modified Landweber method for nonlinear ill-posed operator equations, J. Comput. Appl. Math. 212 (2) (2008) 457–468.
[34] G. Han, G. Qu, M. Jiang, Relaxation strategy for the Landweber method, Signal Process. 125 (2016) 87–96.
[35] D. Garmatter, B. Haasdonk, B. Harrach, A reduced basis Landweber method for nonlinear Inv Prob, Inverse Probl. 32 (3) (2016) 035001.
[36] J. Jang, S. Lee, K. Kim, B. Choi, Modified iterative Landweber method in electrical capacitance tomography, Meas. Sci. Technol. 17 (7) (2006) 1909.
[37] J. Sun, W. Tian, H. Che, S. Sun, S. Gao, L. Xu, W. Yang, Proportional-integral controller modified Landweber iterative method for image reconstruction in electrical capacitance tomography, IEEE Sens. J. 19 (19) (2019) 8790–8802.
[38] M. Burger, E. Resmerita, M. Benning, An entropic Landweber method for linear ill-posed problems, Inverse Probl. 36 (1) (2019) 015009.
[39] Z. Wang, A.C. Bovik, H.R. Sheikh, E.P. Simoncelli, Image quality assessment: from error visibility to structural similarity, IEEE Trans. Image Proc. 13 (4) (2004) 600–612.
[40] X. Zhou, F. Zhou, X. Bai, B. Xue, A boundary condition based deconvolution framework for image deblurring, J. Comput. Appl. Math. 261 (2014) 14–29.
[41] M. Donatelli, C. Estatico, A. Martinelli, S. Serra-Capizzano, Improved image deblurring with anti-reflective boundary conditions and re-blurring, Inverse Probl. 22 (6) (2006) 2035.

Min Zhang, Ph.D., was an Instructor at Department of Radiology, Brigham and Women's Hospital, Harvard Medical School, Boston, MA, USA. She is now with Collaborative Innovation Center of Artificial Intelligence, College of Computer Science and Technology, Zhejiang Universtiy, Hangzhou, Zhejiang, China. Her research interests are in shape analysis, image analysis and processing.

Geoffrey S. Young, MD, is an Associate Professor in the Departments of Radiology of the Brigham and Women's Hospital and Harvard Medical School, Boston, MA, USA. His research interests include medical image analysis and interpretation, image quality, and data analysis.

Yanmei Tie, Ph.D., is an Assistant Professor at Department of Neurosurgery, Brigham and Women's Hospital, Harvard Medical School, Boston, MA, USA. Her research interests are in data modeling and analysis, and algorithm development.

Xianfeng Gu, Ph.D., is a Professor at Department of Computer Science, Stony Brook University, Stony Brook, NY. His research interests are in image processing, conformal geometry, medical imaging, and geometric modeling.

Xiaoyin Xu, Ph.D., is an Associate Professor at Department of Radiology, Brigham and Women's Hospital, Harvard Medical School, Boston, MA, USA. His research interests are in bioinformatics, image processing, and data analysis.